

# Molecular Imaging of Myocardial Fibroblast Activation in Patients with Advanced Aortic Stenosis Before Transcatheter Aortic Valve Replacement: A Pilot Study

Johanna Diekmann\*<sup>1</sup>, Jonas Neuser\*<sup>2</sup>, Manuel Röhrich<sup>3</sup>, Thorsten Derlin<sup>1</sup>, Carolin Zwadlo<sup>2</sup>, Tobias Koenig<sup>2</sup>, Desiree Weiberg<sup>1</sup>, Felix Jäckle<sup>2</sup>, Tibor Kempf<sup>2</sup>, Tobias L. Ross<sup>1</sup>, Jochen Tillmanns<sup>2</sup>, James T. Thackeray<sup>1</sup>, Julian Widder<sup>2</sup>, Uwe Haberkorn<sup>3</sup>, Johann Bauersachs\*<sup>2</sup>, and Frank M. Bengel\*<sup>1</sup>

<sup>1</sup>Department of Nuclear Medicine, Hannover Medical School, Hannover, Germany; <sup>2</sup>Department of Cardiology and Angiology, Hannover Medical School, Hannover, Germany; and <sup>3</sup>Department of Nuclear Medicine, University Hospital Heidelberg, Heidelberg, Germany

Using multimodal imaging, we investigated the extent and functional correlates of myocardial fibroblast activation in patients with aortic stenosis (AS) scheduled for transcatheter aortic valve replacement (TAVR). AS may cause myocardial fibrosis, which is associated with disease progression and may limit response to TAVR. Novel radiopharmaceuticals identify upregulation of fibroblast activation protein (FAP) as a cellular substrate of cardiac profibrotic activity. **Methods:** Twenty-three AS patients underwent <sup>68</sup>Ga-FAP inhibitor 46 (<sup>68</sup>Ga-FAPI) PET, cardiac MRI, and echocardiography within 1–3 d before TAVR. Imaging parameters were correlated and then were integrated with clinical and blood biomarkers. Control cohorts of subjects without a history of cardiac disease and with ( $n = 5$ ) and without ( $n = 9$ ) arterial hypertension were compared with matched AS subgroups. **Results:** Myocardial FAP volume varied significantly among AS subjects (range, 1.54–138 cm<sup>3</sup>, mean  $\pm$  SD, 42.2  $\pm$  35.6 cm<sup>3</sup>) and was significantly higher than in controls with (7.42  $\pm$  8.56 cm<sup>3</sup>,  $P = 0.007$ ) and without (2.90  $\pm$  6.67 cm<sup>3</sup>;  $P < 0.001$ ) hypertension. FAP volume correlated with N-terminal prohormone of brain natriuretic peptide ( $r = 0.58$ ,  $P = 0.005$ ), left ventricular ejection fraction ( $r = -0.58$ ,  $P = 0.02$ ), mass ( $r = 0.47$ ,  $P = 0.03$ ), and global longitudinal strain ( $r = 0.55$ ,  $P = 0.01$ ) but not with cardiac MRI T1 (spin-lattice relaxation time) and extracellular volume ( $P =$  not statistically significant). In-hospital improvement in left ventricular ejection fraction after TAVR correlated with pre-TAVR FAP volume ( $r = 0.440$ ,  $P = 0.035$ ), N-terminal prohormone of brain natriuretic peptide, and strain but not with other imaging parameters. **Conclusion:** FAP-targeted PET identifies varying degrees of left ventricular fibroblast activation in TAVR candidates with advanced AS. <sup>68</sup>Ga-FAPI signal does not match other imaging parameters, generating the hypothesis that it may become useful as a tool for personalized selection of optimal TAVR candidates.

**Key Words:** aortic stenosis; myocardial fibrosis; molecular imaging; fibroblast activation protein; PET

**J Nucl Med 2023; 00:1–8**  
DOI: 10.2967/jnumed.122.265147

**A**dvanced aortic stenosis (AS) is associated with significant morbidity and mortality (1–3). Transcatheter aortic valve replacement (TAVR) is increasingly used, primarily in high-risk patients (4), although a broader use in lower-risk AS has been suggested (5). Myocardial fibrosis is thought to play a critical role in AS, in the response to therapy and in subsequent outcome (6). In TAVR recipients, the histologic severity of myocardial fibrosis varies significantly and independently predicts left ventricular (LV) remodeling and survival (7,8). Accordingly, myocardial fibrosis has emerged as an imaging target in AS. Strain analysis from transthoracic echocardiography (TTE) provides indirect measures of fibrosis in cardiomyopathies (9,10) and in AS (11). In cardiac MRI (CMR), late gadolinium enhancement (LGE) identifies scars and areas of replacement fibrosis (12). Parametric T1 (spin-lattice relaxation time) mapping describes altered tissue composition as an indicator of diffuse interstitial fibrosis (13,14). However, LGE and elevated T1 are, for example, also found in areas with extracellular expansion due to edema or infiltration (12), and T1 may have limited specificity for discriminating AS patients from healthy controls (15).

Recently, specific radioligands for fibroblast activation protein (FAP) have been developed for targeted PET and were initially used to characterize tumor stroma (16). FAP is a membrane-bound serine protease (17,18) that is highly expressed by activated myofibroblasts. In profibrotic conditions, it therefore identifies the biologic activity of tissue fibroblasts as a cell-based mechanism that is distinct from the extracellular matrix. The feasibility of noninvasive PET-based interrogation of cardiac <sup>68</sup>Ga-FAPI expression has, for example, been shown after acute myocardial infarction (19–23). Moreover, among oncologic patients, a less intense but variable myocardial <sup>68</sup>Ga-FAPI signal was proportional to cardiovascular risk factors such as hypertension and diabetes mellitus (24).

We hypothesized that FAP-targeted PET will identify the presence and inter- and intraindividual heterogeneity of myocardial fibroblast activation in AS. We also hypothesized that this signal of profibrotic activity will be distinct from, and thereby complementary to, other imaging parameters that reflect tissue composition. We tested our hypotheses by a comprehensive global and regional integration of multimodality noninvasive imaging parameters and their relation to established clinical risk markers and short-term response to TAVR. We speculate that confirmation of our hypotheses may support the use of FAP-targeted PET in future

Received Nov. 7, 2022; revision accepted Apr. 10, 2023.  
For correspondence or reprints, contact Johanna Diekmann (diekmann.johanna@mh-hannover.de).  
\*Contributed equally to this work.  
Published online Jun. 8, 2023.  
COPYRIGHT © 2023 by the Society of Nuclear Medicine and Molecular Imaging.

studies seeking to optimize candidate selection for TAVR based on their individual fibrotic disease profile.

## MATERIALS AND METHODS

### Study Design and Participants

We included 23 patients (11 men, 12 women; mean age  $\pm$  SD,  $84.1 \pm 3.3$  y) who had undergone clinical evaluation including CMR, TTE, and FAP-targeted PET with  $^{68}\text{Ga}$ -FAP inhibitor 46 ( $^{68}\text{Ga}$ -FAPI) before TAVR at Hannover Medical School. AS had been evaluated, and eligibility for TAVR determined, according to clinical guidelines (25). All patients had classic high-gradient AS and sinus rhythm. Patients equipped with a permanent pacemaker or implantable cardioverter defibrillator and who had severe renal dysfunction (glomerular filtration rate  $< 30$  mL/min), chronic inflammatory disease, or eminent frailty were excluded. All patients gave written informed consent before undergoing imaging. The study was in accordance with the ethical guidelines of the 1975 Declaration of Helsinki, and the local ethical committee approved the project (approval 9553\_BO\_K\_2021).

### Radionuclide Imaging

FAP-targeted PET was conducted 1–3 d before TAVR, using the specific ligand  $^{68}\text{Ga}$ -FAPI-46, which was synthesized in house according to good manufacturing practices as previously described (26) and was used clinically according to §13.2b of the German Pharmaceuticals Act for determination of myocardial profibrotic activity. Static PET images were acquired for 20 min using a Biograph mCT 128 system (Siemens), beginning 60 min after intravenous injection of  $118 \pm 16$  MBq of  $^{68}\text{Ga}$ -FAPI-46. Low-dose CT was used for attenuation correction. Images were iteratively reconstructed, using time-of-flight and point-spread function information (True X; Siemens). Peak and  $\text{SUV}_{\text{mean}}$  were obtained for myocardium, blood pool (left atrium), and other organs (liver, spleen, bone marrow, lungs) using volumes of interest of  $1 \text{ cm}^3$  and commercial software (syngo.via, V50B; Siemens Healthcare). Myocardial FAP volume was determined using an isocontour volume of interest including all voxels above an individually determined threshold (blood pool  $\text{SUV}_{\text{mean}} + 2$  SDs) with exclusion of valve regions. Additionally, the area of FAP upregulation was calculated by polar map analysis as previously described (19). Segmental  $\text{SUV}_{\text{mean}}$  was calculated using the American Heart Association 17-segment model and polar maps. Apical segments were merged for comparability to CMR and echocardiography.

### CMR

CMR was performed using a 1.5-T scanner (Magnetom Avanto; Siemens) in 22 of 23 patients (97%) at 1–4 d before TAVR. In 2 of 22 patients, T1 mapping was not performed because of technical problems. Cine images were obtained using a balanced steady-state free-precession sequence (True FISP; Siemens). Parametric T1 maps were acquired in 3 short-axis slices (basal, midventricular, and apical LV) covering 16 segments (available for 16 patients), using the modified look-locker sequence before and after administration of contrast agent. LGE was imaged by phase-sensitive inversion recovery sequences, 10–15 min after bolus injection of a 0.15 mmol/kg

dose of gadolinium-diethylenetriamine pentaacetate (Gadavist; Bayer Healthcare). Extracellular volume fraction was calculated from myocardial and blood T1 relaxation times before and after contrast administration, using the most recent hematocrit level. Global analysis included determination of LV ejection fraction (LVEF), volumes, mass, and extent of LGE, indexed by body surface area (27). Segmental analysis included native T1 and postcontrast T1 relaxation times, using the 16-segment model. Threshold analysis using the mean + 2 SDs of healthy controls' identified segments with prolonged native T1 relaxation times (28). Cvi42 software (Circle Cardiovascular Imaging) was used.

### TTE

TTE was performed 1–3 d before and after TAVR, using an EPIQ7 equipped with an X5-1 transducer (Philips). LV strain images were recorded using standard apical views. Speckle tracking for measurement of global longitudinal strain and LVEF were assessed offline using a TomTec Imaging Systems ultrasound software. Segmental longitudinal strain was assessed using 18 segments, and 4 apical segments were merged for comparability to CMR and PET. Threshold analysis using the mean + 2 SDs of healthy controls (29) identified segments with impaired longitudinal strain.

### Control Groups

From a historic sample of cancer patients having undergone  $^{68}\text{Ga}$ -FAPI-46 PET for staging at the University of Heidelberg, 2 control groups were identified and matched to AS subgroups by age and sex. Imaging modalities, tracers, and evaluations were identical to the Hannover protocol (image acquisition 60 min after injection). First, a group of 9 control subjects (4 with glioblastoma, 3 with adenoid cystic carcinoma, 1 with pancreas carcinoma, and 1 with a suspected cancerous polyp) was selected and matched 1:2 to 18 AS patients. This group had no history of cardiac disease, cardiotoxic chemotherapy, or radiation therapy of the chest; no coronary calcification; and no known cardiovascular risk factors, including smoking, diabetes mellitus, or

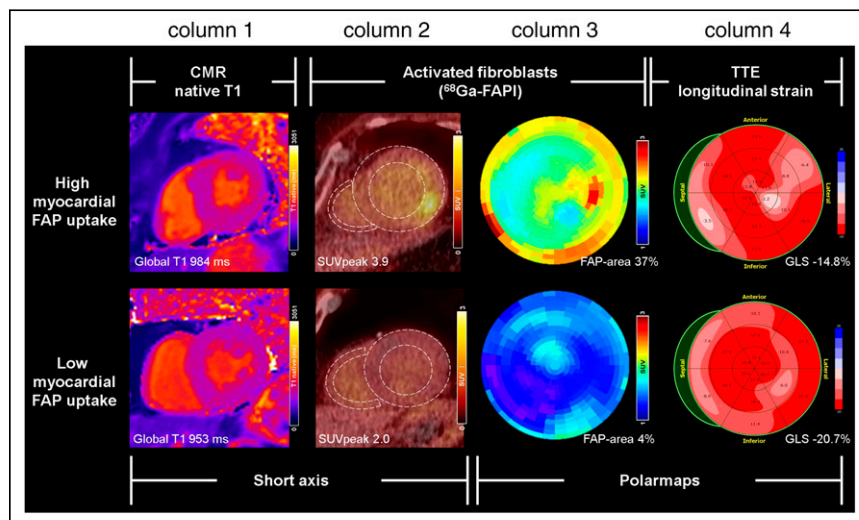


**FIGURE 1.** Multimodal characterization of myocardial fibrosis in AS patients before TAVR. Shown are 2 cases with high and low myocardial  $^{68}\text{Ga}$ -FAPI signal, as indicated by representative midventricular short-axis PET/CT image (column 2) and parametric polar maps of  $^{68}\text{Ga}$ -FAPI uptake (column 3; polar maps are 2-dimensional display of 3-dimensional LV activity with apex in center, base in periphery, anterior wall on top, inferior wall on bottom, septum on left, and lateral wall on right). High  $^{68}\text{Ga}$ -FAPI signal was associated with mild elevation of native T1 from CMR (column 1) and mild reduction of global longitudinal strain at TTE (column 4). Yet, neither CMR T1 nor TTE global longitudinal strain show similarly clear distinction between patients when compared with  $^{68}\text{Ga}$ -FAPI signal. GLS = global longitudinal strain.

**TABLE 1**  
PET Parameters

Variable	All AS patients (n = 23)			Sex-matched AS patients (n = 18)			Oncologic sex-matched controls (n = 9)			Age- and sex-matched AS patients (n = 5)			Oncologic age- and sex-matched controls with AHT (n = 5)		
	Mean ± SD	Range	P	Mean ± SD	Range	P	Mean ± SD	Range	P	Mean ± SD	Range	P	Mean ± SD	Range	P
Area of FAP upregulation (% of LV)	32.0 ± 29.1	0–91		29.6 ± 30.6	0–91		4.44 ± 7.83	0–24	0.004	43.4 ± 20.6	17–68	0.004	9.40 ± 11.2	0–27	0.012
SUV <sub>mean</sub> (of total LV)	2.50 ± 0.43	1.88–3.51		2.58 ± 0.42	1.93–3.51		1.89 ± 0.46	1.44–2.63	<0.001	2.28 ± 0.45	1.81–2.93	<0.001	1.47 ± 0.34	1.12–1.91	0.014
FAP volume (cm <sup>3</sup> )	42.2 ± 35.6	1.54–137.8		37.9 ± 35.4	1.54–137.8		2.90 ± 6.67	0.01–20.62	<0.001	43.1 ± 20.4	23.2–75.9	<0.001	7.42 ± 8.56	0.71–18.3	0.007
Myocardial SUV-to-blood pool ratio	1.87 ± 0.5	1.20–3.15		1.81 ± 0.53	1.09–2.78		1.30 ± 0.56	0.74–2.57	0.030	1.86 ± 0.25	1.44–2.12	0.030	1.47 ± 0.34	1.18–1.99	0.003
Organ <sup>68</sup> Ga-FAPI signal (SUV <sub>peak</sub> )															
Myocardium	3.35 ± 0.91	1.87–5.42		3.46 ± 0.96	1.87–5.42		3.46 ± 0.96	1.21–3.86	<0.001	3.44 ± 0.67	2.48–4.21	<0.001	1.62 ± 0.25	1.41–1.93	<0.001
Spleen	1.39 ± 0.38	0.79–2.12		1.41 ± 0.38	0.79–2.12		1.13 ± 0.25	0.83–1.51	0.052	1.35 ± 0.34	1.05–1.91	0.052	1.01 ± 0.04	0.99–1.06	0.147
Liver	1.33 ± 0.35	0.81–2.64		1.36 ± 0.38	0.81–2.31		1.29 ± 0.67	0.80–3.49	0.731	1.35 ± 0.41	0.99–1.88	0.731	1.41 ± 0.49	0.92–2.12	0.817
Bone marrow	0.90 ± 0.25	1.05–4.05		0.92 ± 0.26	0.43–1.29		0.99 ± 0.27	0.60–1.35	0.540	1.05 ± 0.29	0.74–1.90	0.540	0.78 ± 0.18	0.50–1.00	0.122
Lung	0.58 ± 0.21	0.23–1.13		0.63 ± 0.20	0.35–1.13		0.52 ± 0.33	0.30–1.39	0.326	0.66 ± 0.22	0.54–0.99	0.326	0.56 ± 0.17	0.40–0.74	0.417
Blood pool (left atrium)	1.89 ± 0.30	1.48–2.84		1.94 ± 0.31	1.48–2.84		1.43 ± 0.24	1.20–1.90	<0.001	1.71 ± 0.29	1.64–2.38	<0.001	1.24 ± 0.52	1.41–1.80	0.082

AHT = arterial hypertension.

**TABLE 2**  
CMR

Variable	All patients	All patients indexed (mL/m <sup>2</sup> )
Global function ( <i>n</i> = 22)		
EDV (mL)	118.6 ± 26.7 (83–191)	66.5 ± 12.9 (45.0–102.0)
ESV (mL)	43.5 ± 13.8 (29–84)	24.3 ± 6.8 (15.0–43.0)
SV (mL)	75.2 ± 14.8 (53–119)	42.1 ± 7.0 (30.0–64.0)
LVM (g)	116.2 ± 21.3 (77–157)	66.3 ± 11.9 (40.0–86.0)
LVEF (%)	63.8 ± 4.4 (53–72)	
Global mapping ( <i>n</i> = 20)		
T1 global native (ms)	977.2 ± 25.8 (939–1,049)	
T1 global contrast (ms)	448.8 ± 48.8 (363–539)	
ECV global (%)	28.0 ± 3.9 (22–38)	

ECV = extracellular volume fraction; EDV = end-diastolic volume; ESV = end-systolic volume; SV = stroke volume; LVM = LV mass. Data are mean ± SD and range.

arterial hypertension. Second, 5 control subjects (all with pancreas carcinoma) with arterial hypertension were identified and matched to 5 AS patients.

### Statistical Analysis

Statistical analyses were performed using SPSS, version 27 (IBM), for Microsoft Windows and Prism, version 9 (GraphPad Software). Categorical variables are presented with absolute and relative frequencies. For quantitative continuous variables, testing for a gaussian distribution was performed using Shapiro–Wilk tests. For data with a gaussian distribution, paired Student *t* tests or 1-way ANOVA with Tukey multiple-comparison tests were used depending on the number of compared groups. Paired continuous variables were compared using the Wilcoxon test; nonpaired continuous variables were compared using a 2-sided *t* test. Categorical variables were compared using the  $\chi^2$  test. Nonparametric unpaired data were analyzed with Mann–Whitney *U* tests. Pearson correlation coefficients were calculated for bivariate correlation analyses. All statistical analyses were performed 2-sided, and a *P* value of less than 0.05 was considered to indicate statistical significance.

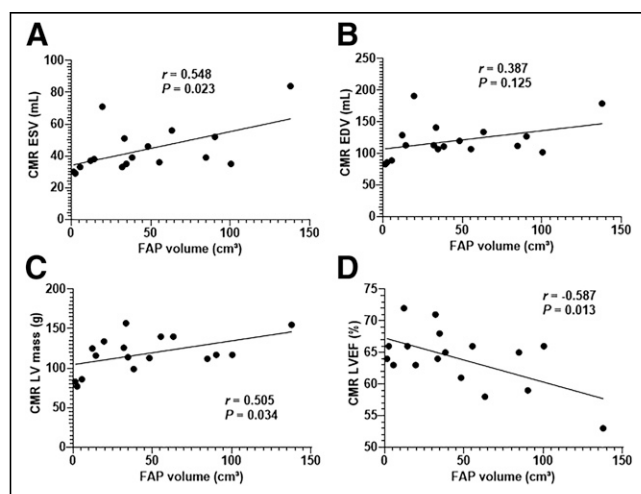


**FIGURE 2.** Regression plot for myocardial volume of elevated <sup>68</sup>Ga-FAPI signal (FAP volume) and LV function parameters derived from CMR: end-systolic volume (A), end-diastolic volume (B), LV mass (C), and LVEF (D). EDV = end-diastolic volume.

### RESULTS

Patient characteristics are summarized in Supplemental Table 1 (supplemental materials are available at <http://jnm.snmjournals.org>). Mean age was 84 ± 3 y, and 52% were female. Most AS patients presented with a high burden of cardiovascular comorbidities (Supplemental Tables 1 and 2).

### Myocardial <sup>68</sup>Ga-FAPI Signal Is Elevated in AS and Shows Inter- and Intraindividual Variability

A wide range of myocardial <sup>68</sup>Ga-FAPI signal patterns was detected in the AS cohort (Fig. 1; Table 1). The area of significant FAP upregulation versus the blood pool ranged from 0% to 91% of the left ventricle (median, 20.0%; interquartile range, 4.0%–58.0%; Supplemental Fig. 1). Similarly, the global volume of elevated <sup>68</sup>Ga-FAPI signal displayed high variance among patients, with a range of 1.5–138 cm<sup>3</sup> (median, 33.4 cm<sup>3</sup>; interquartile range, 14.4–63.3 cm<sup>3</sup>). Mean myocardial SUV as a measure of <sup>68</sup>Ga-FAPI signal intensity ranged from 1.9 to 3.5 (SUV<sub>mean</sub>, 2.5 ± 0.4). Interindividual regional LV distribution patterns were highly variable, whereas basal myocardial regions were more frequently involved.

Myocardial FAP volume was significantly higher in AS patients than in controls without hypertension (37.9 ± 35.4 cm<sup>3</sup> vs. 2.90 ± 6.67 cm<sup>3</sup>, *P* < 0.001; Table 1; Supplemental Fig. 2). The area of FAP upregulation, SUV<sub>mean</sub>, and SUV<sub>peak</sub> of the total left ventricle were equally higher in AS patients (*P* < 0.001 each). Additionally, matched comparison with hypertensive controls also showed that FAP volume was significantly higher in AS patients (43.1 ± 20.4 cm<sup>3</sup> vs. 7.42 ± 8.56 cm<sup>3</sup>, *P* < 0.001; Supplemental Fig. 2).

### <sup>68</sup>Ga-FAPI Signal Elevation Is Specific to Myocardium in AS

Signal intensity was very low in the blood pool, albeit slightly higher in AS than in controls (1.94 ± 0.31 vs. 1.43 ± 0.24, *P* < 0.001), confirming the feasibility of detecting mild <sup>68</sup>Ga-FAPI signal elevation in the heart. Additionally, no elevated signal and no difference between AS and controls was identified in potential networking organs such as lung, liver, spleen, and bone marrow, suggesting that profibrotic activity in AS is specific to the myocardium (Table 1). No significant correlation between myocardial <sup>68</sup>Ga-FAPI signal and the SUV of other organs was detected (Supplemental Fig. 3).

**TABLE 3**  
TTE and TAVR Procedure

Variable	Data
LVEF (% , 2-dimensional)	60.1 ± 5.9 (44–70)
LVEF (% , 2-dimensional) after TAVR	61.8 ± 3.7 (57–72)
Transaortic gradient (mm Hg, maximum)	79.0 ± 13.6 (54–110)
Transaortic gradient (mm Hg, mean)	50.4 ± 8.1 (38–70)
Aortic regurgitation	7 (30.4)
AVA (cm <sup>2</sup> )	0.68 ± 0.18 (0.37–0.95)
THV SAPIEN (Edwards Lifesciences)	14 (60.9)
THV CoreValve (Medtronic)	9 (39.1)
Device success	23 (100)
New permanent pacemaker	1 (4.3)

AVA = aortic valve area; THV = transcatheter heart valve.  
Qualitative data are number and percentage (*n* = 23); continuous data are mean ± SD and range.

**Global Myocardial <sup>68</sup>Ga-FAPI Signal Correlates with Markers of Heart Failure Severity in AS**

FAP volume significantly correlated with the levels of serum N-terminal prohormone of brain natriuretic peptide (*r* = 0.58, *P* = 0.004; Supplemental Fig. 4). No other correlations between <sup>68</sup>Ga-FAPI imaging parameters and blood biomarkers were observed. CMR parameters are summarized in Table 2. Of note, FAP volume correlated significantly with volume, LV mass, and LVEF (all *P* < 0.05; Fig. 2; Supplemental Fig. 5). No significant correlations between FAP volume and global mapping parameters could be detected (T1 global native: *r* = -0.058, *P* = 0.804; T1 global contrast: *r* = -0.143, *P* = 0.525, extracellular volume fraction global: *r* = 0.011, *P* = 0.990).

Also, TTE was available for all patients before and after TAVR (in-hospital follow-up, Table 3). Mean aortic valve area was severely reduced (0.68 ± 0.18 cm<sup>2</sup>, severe AS < 1 cm<sup>2</sup>) (30), and mean transaortic pressure gradient was severely increased (50.4 ± 8.1 mmHg, severe AS > 40 mmHg) (30) before TAVR. FAP volume

significantly correlated with TTE-derived cardiac function (Fig. 3), including LVEF before TAVR (*r* = -0.58, *P* = 0.012) and LV global longitudinal strain (*r* = 0.58, *P* = 0.012) and tended to correlate with the mean transaortic gradient (*r* = 0.44, *P* = 0.07).

**Segmental <sup>68</sup>Ga-FAPI Signal Is Not Identical to Other Imaging Markers of Fibrosis in AS**

In total, 299 segments with complete data from PET, CMR, and TTE were analyzed. Segmental <sup>68</sup>Ga-FAPI SUV<sub>mean</sub> was significantly higher in basal than in midventricular (*P* [ANOVA] = 0.022) and apical segments (*P* [ANOVA] = 0.034, Fig. 4). Segmental SUV<sub>mean</sub> correlated weakly but significantly with segmental longitudinal strain from TTE (*r* = 0.119, *P* = 0.002; Supplemental Fig. 6), native T1 (*r* = 0.271, *P* < 0.001), and postcontrast T1 from CMR (*r* = -0.330, *P* < 0.001). To define <sup>68</sup>Ga-FAPI signal elevation in a segment, an SUV<sub>mean</sub> more than 2 SDs above the blood pool level was chosen. This yielded 110 of 299 segments (37%) as <sup>68</sup>Ga-FAPI-positive (Fig. 5). The native T1 relaxation time was mildly but significantly longer in the <sup>68</sup>Ga-FAPI-positive segments (973 ± 35 vs. 961 ± 37 ms for <sup>68</sup>Ga-FAPI-negative, *P* = 0.015), and longitudinal strain was mildly but significantly reduced (-13.0 ± 7.1 vs. -16.0% ± 8.4%, *P* = 0.003) in <sup>68</sup>Ga-FAPI-positive segments. Also, 19 of 299 segments (6%) showed LGE, but only 11 of 19 (58%) segments with LGE were <sup>68</sup>Ga-FAPI-positive. There was a relevant mismatch between <sup>68</sup>Ga-FAPI positivity and elevated T1 at CMR (congruent signal in 51/110 segments), as well as impaired longitudinal strain at TTE (congruent signal in 78/110 segments), suggesting that the 3 modalities do not identify the same components of the fibrotic process.

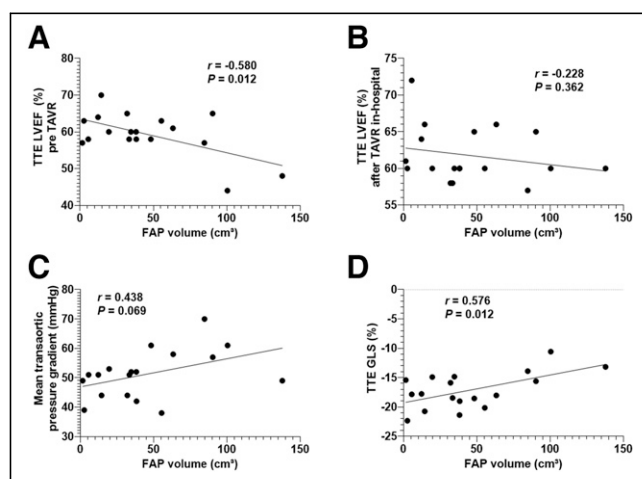


**FIGURE 3.** Regression plot for myocardial volume of elevated <sup>68</sup>Ga-FAPI signal (FAP volume) and LV function parameters derived from TTE: LVEF before TAVR (A), LVEF after TAVR (B), mean transaortic gradient (C), and global longitudinal strain (D). GLS = global longitudinal strain.

**<sup>68</sup>Ga-FAPI Signal Is Predictive of Short-Term Change in LVEF After TAVR**

After TAVR, LVEF did not change significantly in

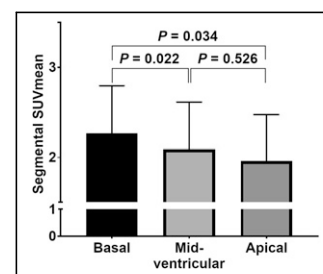


**FIGURE 4.** Segmental analysis: SUV<sub>mean</sub> of <sup>68</sup>Ga-FAPI ligand at PET was significantly higher in basal than midventricular and distal myocardial segments.

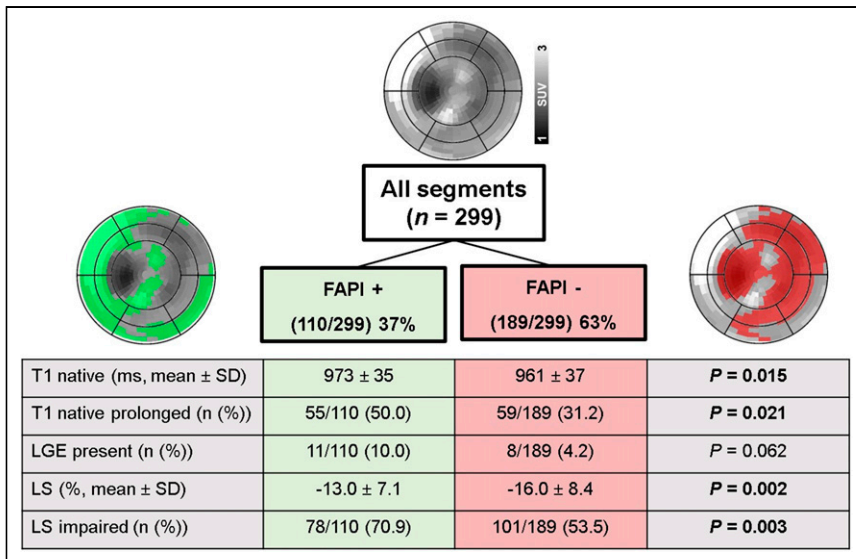


**FIGURE 5.** Classification of segments into  $^{68}\text{Ga}$ -FAPI-upregulated (FAPI+) and  $^{68}\text{Ga}$ -FAPI-negative segments (FAPI-) when compared with blood pool background signal, illustrated by patient example (polar map). Native T1 relaxation time was significantly longer in  $^{68}\text{Ga}$ -FAPI-positive segments. More LGE was found in  $^{68}\text{Ga}$ -FAPI-positive segments, and global longitudinal strain was significantly impaired in  $^{68}\text{Ga}$ -FAPI-positive segments. Yet, agreement between  $^{68}\text{Ga}$ -FAPI, T1, and longitudinal strain elevation was only partial. FAPI+ =  $^{68}\text{Ga}$ -FAPI-upregulated; FAPI- =  $^{68}\text{Ga}$ -FAPI-negative; LS = longitudinal strain.

the entire group ( $60.1\% \pm 5.9\%$  vs.  $61.8\% \pm 3.7\%$  before,  $P = 0.19$ ). Individually, however, in-hospital LVEF improvement significantly correlated with myocardial FAP volume ( $r = 0.440$ ,  $P = 0.035$ ), N-terminal prohormone of brain natriuretic peptide ( $r = 0.480$ ,  $P = 0.024$ ), and global longitudinal strain ( $r = 0.440$ ,  $P = 0.013$ ; Fig. 6). No correlation between in-hospital LVEF improvement and other parameters from CMR or TTE was observed.

## DISCUSSION

AS is the most common valvular disease in the Western world, and early treatment is recommended in symptomatic patients (25). However, symptoms often occur late, after adverse cardiac remodeling has led to overt heart failure. Progressive valve narrowing causing an increased afterload, along with adaptive LV hypertrophy, facilitates the transition to heart failure (6,31). It is thought that myocyte death and interstitial fibrosis are key mechanisms in this transformation (32). With new  $^{68}\text{Ga}$ -FAPI tracers, imaging of activated fibroblasts is now feasible. In oncologic patients, myocardial FAP upregulation was incidentally identified and associated with preexisting cardiovascular comorbidities (33). More recently, further studies have

demonstrated the feasibility of myocardial  $^{68}\text{Ga}$ -FAPI imaging, particularly after acute myocardial infarction (19,20,22–24). A strong and specific  $^{68}\text{Ga}$ -FAPI signal was detected in the infarct region, where fibroblasts need to form a robust scar. Yet, in addition to this area of replacement fibrosis, there was also an elevated  $^{68}\text{Ga}$ -FAPI signal in viable periinfarct tissue, as a possible substrate for development of interstitial fibrosis. Ex vivo analysis of human heart tissue identified significant  $^{68}\text{Ga}$ -FAPI expression in the LV tissue of failing hearts, whereas normal hearts had minimal  $^{68}\text{Ga}$ -FAPI expression (34). Thus, FAP is a suitable target marker of activated cardiac fibroblasts, and  $^{68}\text{Ga}$ -FAPI radioligands (16,26) are promising for noninvasive detection. Our study was the first, to our knowledge, to describe high inter- and intraindividual heterogeneity for myocardial  $^{68}\text{Ga}$ -FAPI uptake patterns in AS patients before TAVR. Expectedly  $^{68}\text{Ga}$ -FAPI uptake was not as intense and not as extensive as in patients with acute myocardial infarction but was significantly higher than in our matching controls, indicating that the myocardial  $^{68}\text{Ga}$ -FAPI signal is not caused primarily by the presence of cardiovascular comorbidities. Nevertheless, there were various regional distribution patterns and differences between individuals. These differences help to generate a hypothesis that the range of  $^{68}\text{Ga}$ -FAPI signal may be associated with the benefit from TAVR, which is known to be variable (25). Of note, a higher myocardial FAP volume led to a greater direct improvement of in-hospital LVEF after TAVR. This finding is somewhat unexpected, as more severe fibrosis is thought to inhibit LVEF improvement. It should be considered, however, that  $^{68}\text{Ga}$ -FAPI signal identifies not the extracellular matrix component of fibrosis but rather the activation state of fibroblasts as the cellular substrate of profibrotic activity. FAP elevation may potentially reflect a more dynamic remodeling process that involves reversible fibrotic cell activity, as opposed to a burnt-out chronic fibrotic state including irreversible scarring. However, because of the study design, our interpretations need to be verified by prospective studies and should be considered hypothesis-generating at this point.

Interestingly, in our patient cohort, higher preprocedural levels of N-terminal prohormone of brain natriuretic peptide significantly correlated with a greater global volume of fibroblast activation, which supports the possibility that FAP-targeted imaging has potential value as a prognostic biomarker. Globally, the PET results also correlated with functional measures and markers of extracellular matrix expansion and stiffness from CMR and TTE, but no exact regional matching—such as with LGE and T1 relaxation times and longitudinal strain—was detected. T1 relaxation times (28) and extracellular volume fraction (35) were in the expected range for this cohort. The underlying reason for these findings remains uncertain. Targeted imaging of activated fibroblasts

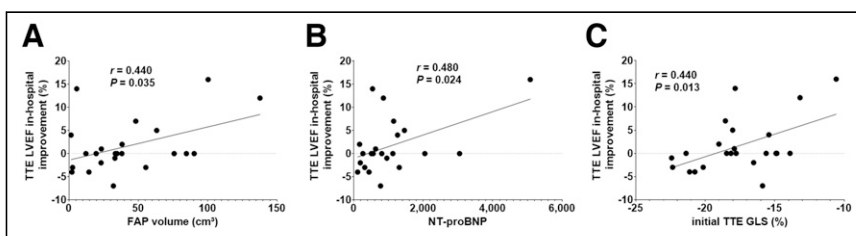


**FIGURE 6.** Regression plot for in-hospital LVEF improvement in percentage and myocardial volume of elevated  $^{68}\text{Ga}$ -FAPI signal (FAP volume) (A), preprocedural levels of N-terminal prohormone of brain natriuretic peptide (B), and preprocedural global longitudinal strain (%) (C). GLS = global longitudinal strain; NT-proBNP = N-terminal prohormone of brain natriuretic peptide.

may be a complementary asset with potential prognostic value in a multimodal fibrosis imaging toolbox and may be further explored for guidance of existing and novel therapies in AS.

Some limitations of this study should be considered. First, the patient population was small, consistent with the hypothesis-generating nature of this early observational project. Indeed, patients were carefully selected to derive a homogeneous cohort without low-flow, low-gradient AS. Another focus was the availability of all imaging modalities, thereby excluding subjects with implantable cardioverter defibrillators, reduced glomerular filtration rate, arrhythmia, or poor TTE windows. Second, because patients had significant cardiovascular comorbidities, myocardial  $^{68}\text{Ga}$ -FAPI signal may have been affected by other factors, including preexisting cardiovascular medication. Coronary angiography and CMR ruled out ischemic cardiomyopathy and cardiac amyloidosis in all patients; however, 48% of patients had preexisting coronary artery disease. Ultimately, effects on cardiac fibroblast activation cannot be ruled out. Yet, this reflects the expected clinical reality of AS before TAVR, and the heterogeneity of observed  $^{68}\text{Ga}$ -FAPI signals provides a foundation for testing prognostic value in larger samples in future projects. Third, PET, CMR, and TTE were performed at different time points using different systems. Coregistration was performed as thoroughly as possible, but slight local mismatches cannot be completely ruled out. Last, a longer-term follow-up after TAVR was not available and will have to be a focus of larger-sample subsequent projects to explore whether TAVR can be guided by  $^{68}\text{Ga}$ -FAPI imaging. Lastly, the matching control patients from our collaborating site in Heidelberg were oncologic patients undergoing  $^{68}\text{Ga}$ -FAPI PET for staging without in-depth information on severity or a detailed individual history of cardiovascular comorbidities. Cardiovascular diagnoses were retrospectively obtained from medical records.

## CONCLUSION

Molecular imaging identifies globally and regionally heterogeneous fibroblast activation in the LV myocardium of patients with severe AS. The  $^{68}\text{Ga}$ -FAPI signal correlates with LV dysfunction and altered extracellular matrix composition, but the FAPI-PET signal remains a distinct imaging biomarker that cannot be replaced by other clinical, blood, or imaging parameters. The present work provides a stimulus for subsequent studies focusing on strategies for image-guided therapy in AS, including fibroblast activation-targeted assays.

## DISCLOSURE

This work was supported by the Deutsche Forschungsgemeinschaft (DFG, Clinical Research Unit KFO 311 [Johann Bauersachs and Frank Bengel] and the Clinician Scientist Program PRACTIS [Johanna Diekmann]), the Leducq Foundation (Transatlantic Network “Immunofib” [Frank Bengel, James Thackeray, and Johanna Diekmann]), and “REBIRTH—Research Center for Translational Regenerative Medicine” (State of Lower Saxony [James Thackeray, Johann Bauersachs, and Frank Bengel]). Uwe Haberkorn has a patent application for quinolone-based FAP-targeting agents for imaging and therapy in nuclear medicine and has shares of a consultancy group for iTheragnostics outside the submitted work. No other potential conflict of interest relevant to this article was reported.

## ACKNOWLEDGMENT

Precursor for  $^{68}\text{Ga}$ -FAPI-46 was kindly provided by Uwe Haberkorn.

## KEY POINTS

**QUESTION:** Is FAP-targeted PET a valuable marker of individual profibrotic activity in patients with AS, and is the PET signal linked to TAVR response?

**PERTINENT FINDINGS:** Using a multimodality, multiparametric correlative analysis, this cross-sectional, observational cohort study confirmed that noninvasive imaging of fibroblast activation in the myocardium of patients with advanced AS is feasible using the radiotracer  $^{68}\text{Ga}$ -FAPI-46 and targeted PET. The severity and regional pattern of fibroblast activation were heterogeneous among patients, and higher FAP volumes determined greater direct functional improvement immediately after TAVR.

**IMPLICATIONS FOR PATIENT CARE:** The observed heterogeneity of fibroblast activation provides a foundation for further studies testing its role as a predictor of outcome and response to valvular replacement or other therapies. The novel imaging assay may be integrated with other imaging and blood biomarkers for a future concept of fibrosis-targeted, image-guided therapeutic decision-making in AS.

## REFERENCES

1. Rosenhek R, Zilberszac R, Schemper M, et al. Natural history of very severe aortic stenosis. *Circulation*. 2010;121:151–156.
2. Coffey S, Cox B, Williams MJ. The prevalence, incidence, progression, and risks of aortic valve sclerosis: a systematic review and meta-analysis. *J Am Coll Cardiol*. 2014;63:2852–2861.
3. Généreux P, Stone GW, O’Gara PT, et al. Natural history, diagnostic approaches, and therapeutic strategies for patients with asymptomatic severe aortic stenosis. *J Am Coll Cardiol*. 2016;67:2263–2288.
4. Vahanian A, Beyersdorf F, Praz F, et al. 2021 ESC/EACTS guidelines for the management of valvular heart disease. *Eur Heart J*. 2022;43:561–632.
5. Ullah W, Gowda SN, Khan MS, et al. Early intervention or watchful waiting for asymptomatic severe aortic valve stenosis: a systematic review and meta-analysis. *J Cardiovasc Med (Hagerstown)*. 2020;21:897–904.
6. Dweck MR, Boon NA, Newby DE. Calcific aortic stenosis: a disease of the valve and the myocardium. *J Am Coll Cardiol*. 2012;60:1854–1863.
7. Herrmann S, Fries B, Salinger T, et al. Myocardial fibrosis predicts 10-year survival in patients undergoing aortic valve replacement. *Circ Cardiovasc Imaging*. 2018;11:e007131.
8. Puls M, Beuthner BE, Topci R, et al. Impact of myocardial fibrosis on left ventricular remodelling, recovery, and outcome after transcatheter aortic valve implantation in different haemodynamic subtypes of severe aortic stenosis. *Eur Heart J*. 2020;41:1903–1914.
9. Pagourelas ED, Mirea O, Duchenne J, et al. Speckle tracking deformation imaging to detect regional fibrosis in hypertrophic cardiomyopathy: a comparison between 2D and 3D echo modalities. *Eur Heart J Cardiovasc Imaging*. 2020;21:1262–1272.
10. Krämer J, Niemann M, Liu D, et al. Two-dimensional speckle tracking as a non-invasive tool for identification of myocardial fibrosis in Fabry disease. *Eur Heart J*. 2013;34:1587–1596.
11. Hoffmann R, Altiok E, Friedman Z, Becker M, Frick M. Myocardial deformation imaging by two-dimensional speckle-tracking echocardiography in comparison to late gadolinium enhancement cardiac magnetic resonance for analysis of myocardial fibrosis in severe aortic stenosis. *Am J Cardiol*. 2014;114:1083–1088.
12. Bing R, Cavalcanti JL, Everett RJ, Clavel MA, Newby DE, Dweck MR. Imaging and impact of myocardial fibrosis in aortic stenosis. *JACC Cardiovasc Imaging*. 2019;12:283–296.
13. Puntmann VO, Peker E, Chandrasekhar Y, Nagel E. T1 Mapping in characterizing myocardial disease: a comprehensive review. *Circ Res*. 2016;119:277–299.

14. Messroghli DR, Moon JC, Ferreira VM, et al. Clinical recommendations for cardiovascular magnetic resonance mapping of T1, T2, T2\* and extracellular volume: a consensus statement by the Society for Cardiovascular Magnetic Resonance (SCMR) endorsed by the European Association for Cardiovascular Imaging (EACVI). *J Cardiovasc Magn Reson*. 2017;19:75.
15. Podlesnikar T, Delgado V, Bax JJ. Cardiovascular magnetic resonance imaging to assess myocardial fibrosis in valvular heart disease. *Int J Cardiovasc Imaging*. 2018;34:97–112.
16. Kratochwil C, Flechsig P, Lindner T, et al. <sup>68</sup>Ga-FAPI PET/CT: tracer uptake in 28 different kinds of cancer. *J Nucl Med*. 2019;60:801–805.
17. Tillmanns J, Hoffmann D, Habbaba Y, et al. Fibroblast activation protein alpha expression identifies activated fibroblasts after myocardial infarction. *J Mol Cell Cardiol*. 2015;87:194–203.
18. Furtado MB, Nim HT, Boyd SE, Rosenthal NA. View from the heart: cardiac fibroblasts in development, scarring and regeneration. *Development*. 2016;143:387–397.
19. Diekmann J, Koenig T, Zwadlo C, et al. Molecular imaging identifies fibroblast activation beyond the infarct region after acute myocardial infarction. *J Am Coll Cardiol*. 2021;77:1835–1837.
20. Kessler L, Kupusovic J, Ferdinandus J, et al. Visualization of fibroblast activation after myocardial infarction using <sup>68</sup>Ga-FAPI PET. *Clin Nucl Med*. 2021;46:807–813.
21. Notohamiprodjo S, Nekolla SG, Robu S, et al. Imaging of cardiac fibroblast activation in a patient after acute myocardial infarction using <sup>68</sup>Ga-FAPI-04. *J Nucl Cardiol*. 2022;29:2254–2261.
22. Varasteh Z, Mohanta S, Robu S, et al. Molecular imaging of fibroblast activity after myocardial infarction using a <sup>68</sup>Ga-labeled fibroblast activation protein inhibitor, FAPI-04. *J Nucl Med*. 2019;60:1743–1749.
23. Diekmann J, Koenig T, Thackeray JT, et al. Cardiac fibroblast activation in patients early after acute myocardial infarction: integration with magnetic resonance tissue characterization and subsequent functional outcome. *J Nucl Med*. 2022;63:1415–1423.
24. Siebermair J, Kohler MI, Kupusovic J, et al. Cardiac fibroblast activation detected by Ga-68 FAPI PET imaging as a potential novel biomarker of cardiac injury/remodeling. *J Nucl Cardiol*. 2021;28:812–821.
25. Vahanian A, Beyersdorf F, Praz F, et al. 2021 ESC/EACTS guidelines for the management of valvular heart disease. *EuroIntervention*. 2022;17:e1126–e1196.
26. Loktev A, Lindner T, Burger EM, et al. Development of fibroblast activation protein-targeted radiotracers with improved tumor retention. *J Nucl Med*. 2019;60:1421–1429.
27. Kawel-Boehm N, Maceira A, Valsangiacomo-Buechel ER, et al. Normal values for cardiovascular magnetic resonance in adults and children. *J Cardiovasc Magn Reson*. 2015;17:29.
28. Bull S, White SK, Piechnik SK, et al. Human non-contrast T1 values and correlation with histology in diffuse fibrosis. *Heart*. 2013;99:932–937.
29. Sugimoto T, Dulgheru R, Bernard A, et al. Echocardiographic reference ranges for normal left ventricular 2D strain: results from the EACVI NORRE study. *Eur Heart J Cardiovasc Imaging*. 2017;18:833–840.
30. Baumgartner H, Hung J, Bermejo J, et al. Recommendations on the echocardiographic assessment of aortic valve stenosis: a focused update from the European Association of Cardiovascular Imaging and the American Society of Echocardiography. *J Am Soc Echocardiogr*. 2017;30:372–392.
31. Chin CWL, Everett RJ, Kwiecinski J, et al. Myocardial fibrosis and cardiac decompensation in aortic stenosis. *JACC Cardiovasc Imaging*. 2017;10:1320–1333.
32. Hein S, Aron E, Kostin S, et al. Progression from compensated hypertrophy to failure in the pressure-overloaded human heart: structural deterioration and compensatory mechanisms. *Circulation*. 2003;107:984–991.
33. Heckmann MB, Reinhardt F, Finke D, et al. Relationship between cardiac fibroblast activation protein activity by positron emission tomography and cardiovascular disease. *Circ Cardiovasc Imaging*. 2020;13:e010628.
34. Aghajanian H, Kimura T, Rurik JG, et al. Targeting cardiac fibrosis with engineered T cells. *Nature*. 2019;573:430–433.
35. Nagaraju CK, Dries E, Popovic N, et al. Global fibroblast activation throughout the left ventricle but localized fibrosis after myocardial infarction. *Sci Rep*. 2017;7:10801.